Experimental Demonstration of a *W*-Band Gyroklystron Amplifier

M. Blank, B. G. Danly, B. Levush, P. E. Latham,* and D. E. Pershing†

Naval Research Laboratory, Code 6840, Washington, D.C. 20375

(Received 27 May 1997)

The experimental demonstration of a four cavity *W*-band (93 GHz) gyroklystron amplifier is reported. The gyroklystron has produced 67 kW peak output power and 28% efficiency in the TE_{011} mode using a 55 kV, 4.3 A electron beam. The full width at half maximum instantaneous bandwidth is greater than 460 MHz, a significant increase over the bandwidth demonstrated in previous *W*-band gyroklystron amplifier experiments. The amplifier is unconditionally stable at this operating point. Experimental results are in good agreement with theoretical predictions. [S0031-9007(97)04699-1]

PACS numbers: 84.40.Fe

The continuing need for high power sources of microwave and millimeter wave radiation for such varied applications as high resolution radars, linear accelerators [1], magnetic resonance imaging [2], and communications has led to extensive research on gyroklystron amplifiers [3–10]. Much like a conventional klystron, the gyroklystron consists of several resonant cavities separated by drift sections cut off to the operating mode. As evidenced in numerous experiments, the interaction of the beam with the trapped mode in the cavity, based on the electron cyclotron maser instability, can reliably and efficiently generate high power, moderate bandwidth electromagnetic radiation at microwave and millimeter wave frequencies. For example, a three cavity *C*-band gyroklystron amplifier produced 54 kW peak output power and 30% efficiency in the TE_{101} at 4.5 GHz [3]. The saturated gain was 30 dB and the FWHM bandwidth was 0.4%. A three cavity *X*-band gyroklystron achieved 16 kW peak output power and 45% efficiency with a FWHM bandwidth of 1% [4]. Fundamental and second harmonic two cavity gyroklystron amplifiers at 9.87 and 19.7 GHz, designed as drivers for linear colliders, achieved peak output powers of 20 and 30 MW, respectively, with efficiencies near 30% [5,6]. A two cavity Ka-band gyroklystron, developed for radar applications, produced 750 kW at 35 GHz in the TE_{021} mode at 24% efficiency [8]. In *W*-band, a pulsed four cavity gyroklystron amplifier achieved 65 kW peak output power at 26% efficiency with 300 MHz bandwidth [9]. A continuous wave version of the device demonstrated 2.5 kW average output power.

The gyroklystron interaction, which takes place in standing wave cavities, inherently gives high efficiency, gain, and output power, but lower bandwidth than devices which rely on traveling wave interactions, such as the gyro-traveling-wave tube (gyro-TWT). Obtaining wider bandwidth without the concomitant problems of the absolute instability associated with the gyro-TWT interaction is an important area of study. It is the goal of the present work to demonstrate a high power, high gain, efficient, stable *W*-band gyroklystron amplifier with greater bandwidth than previously achieved, and to elucidate the basic physics of gyroamplifiers by comparing theoretical predictions with experimental results.

This paper presents an experimental study of a four cavity *W*-band gyroklystron amplifier operating in the TE_{011} mode near the fundamental cyclotron frequency, $\Omega_c = eB/m\gamma$. The circuit consists of a drive cavity, two idler cavities, and an output cavity. The circuit was designed with a time-dependent version of the nonlinear code MAGYKL [11]. The wave equation solved in MAGYKL is given by

$$\frac{da}{dt} + \left(\frac{1}{2} + i\Delta_\omega\right)a = -\frac{QI_b}{2\omega W_{\mathrm{EM}}}\int d\xi \times \frac{c}{\omega}\left\langle \frac{\nu_{\mathrm{perp}} \cdot \mathbf{E}_c e^{-i\omega t}}{\nu_z}\right\rangle, \quad (1)$$

where a is the complex amplitude of the fields, $\Delta_\omega = Q\{\mathrm{Re}\{\omega_c\} - \omega\}/\omega$ is the normalized frequency shift, Q is the quality factor of the cavity, ω is the drive frequency, ω_c is the cold resonant frequency, I_b is the beam current, W_{EM} is the stored energy, c is the speed of light, ν_{perp} and ν_z are the perpendicular and axial electron velocities, $\mathbf{E}_c$ is the cold cavity electric field, and t is the time normalized to Q/ω, i.e., $\omega t/Q$.

In the formulation, the cavities are modeled by a series of straight uniform sections with abrupt discontinuities at the boundaries. This model is strictly accurate for the intermediate cavities, and the up taper of the output cavity is divided into 80 steps to approximate the smooth taper in radius. The fields in each section, expanded as a radial series of TE, TM, and TEM modes, are determined through a scattering matrix solution [12]. Theoretical studies have shown that it is necessary to include many terms in this radial mode series to correctly determine the resonant frequency of the cavity. In order to accurately predict the bandwidth of the amplifier, the formulation detailed in Ref. [11] was modified to include a frequency dependent drive power, as dictated by the resonant frequency and Q of the input cavity. The field amplitude in the drive cavity is given by

$$|a|^2 W_{\mathrm{EM}} = P_{\mathrm{in}} \frac{\omega}{Q_{\mathrm{ext}}} \frac{1}{\left|\omega - \omega_c + \frac{i\omega}{2}\left(\frac{1}{Q_{\mathrm{ext}}} + \frac{1}{Q_{\mathrm{Ohmic}}}\right) + \frac{1}{a}\frac{I_b}{2W_{\mathrm{EM}}}\int d\xi \frac{c}{\omega}\left\langle \frac{\nu_{\mathrm{perp}}\cdot \mathbf{E}_c e^{-i\omega t}}{\nu_z}\right\rangle\right|}, \quad (2)$$

where P_{in} is the input power.

The theoretical model was used to design the interaction circuit and determine the parameters of each cavity, which are summarized in Table I. The drive power is coupled into the circuit through a coaxial cavity similar to that described in [13]. A single cylindrical waveguide excites the TE_{411} mode of the outer cavity. Power is then coupled from the TE_{411} mode in the outer cavity to the TE_{011} mode in the inner cavity through four slots positioned symmetrically around the azimuth of the cavity. The coaxial cavity was analyzed with a finite element electromagnetics code, HFSS, and found to have a resonant frequency of 93.00 GHz, with $Q_{\mathrm{ext}} = 150$ and $Q_{\mathrm{Ohmic}} = 800$, assuming twice the resistivity of ideal stainless steel. HFSS simulations show that approximately 75% of the energy is stored in the TE_{411} mode and 25% is stored in the TE_{011} inner cavity mode at a drive frequency of 93.35 GHz; this power ratio is nearly constant over the operational frequency range.

Because the second and third cavities are terminated by drift sections that are cut off for the TE_{011} mode at 93 GHz, the diffractive Q's are quite large. The design Q's of 175 are achieved through dielectric loading of the cavities. The scattering matrix formulation described in [12] was modified to include dielectric materials and used to predict resonant frequencies and Q's of the loaded idler cavities. The second and third cavities are designed to have cold resonant frequencies that are stagger tuned around the frequency of the output cavity in order to enhance the bandwidth of the amplifier. The output cavity consists of a straight section followed by an iris which is cut off to the TE_{011} mode at 93 GHz, and a linear up taper to the collector radius. The wave is coupled out diffractively, and there is no ceramic loading the output cavity. The first and second cutoff drift lengths are loaded only by the dielectrics on the upstream walls of the idler cavities, and the drift length separating the penultimate cavity and output cavity is unloaded.

A linear theory analysis [14] was used to determine the stability of each cavity and drift section for the nominal operating parameters, a 55 kV beam with velocity ratio $\alpha = \nu_{\mathrm{perp}}/\nu_z = 1.5$ and a perpendicular velocity spread of 9%. The magnetic field value was chosen so that the drive cavity is run in the positive beam loading regime, where the efficiency is negative. Therefore, the input cavity is stable in the TE_{011} operating mode. At the operating point, the beam loaded Q factor, which is proportional to the real part of the last term in the denominator of Eq. (2), is $Q_b = 1350$. According to the linear theory, other modes, including the TE_{012}, TE_{112}, and TE_{211} modes, have start oscillation currents approaching 100 A and are not expected to oscillate. In the intermediate cavities, the mode with the minimum start oscillation current is TE_{211} at 100 GHz. The theoretical start current was found to be 12 A, which is significantly higher than the operating current. In the output cavity, the TE_{011} mode has a theoretical minimum start oscillation current of 3 A at a magnetic field 10% below the desired operating field, 35.8 kG. The TE_{211} mode at 100 GHz in the unloaded drift section was found to have a minimum start current of approximately 10 A.

The circuit was built and cold tested on a vector network analyzer. The cavities were excited and sampled through two holes positioned 180° apart in the side wall. The transmission spectra for the idler and output cavities, measured in air, are shown in Fig. 1. The cold resonant frequencies of the cavities in vacuum will be 30 MHz higher than the values determined in air due to the dielectric constant of air at standard temperature and pressure. The measured resonant frequencies, adjusted

TABLE I. Summary of design values and cold test results for the four interaction cavities. The cold resonant frequencies under vacuum will be 30 MHz higher than the cold test values determined in air due to the dielectric constant of air at standard temperature and pressure.

		Design		Cold test	
	L (cm)	f_0 (GHz)	Q_L	$f_{0\,\mathrm{vac}}$ (GHz)	Q_L
Cavity 1	0.43	93.00	125		...
Cavity 2	0.50	93.52	175	93.59	130
Cavity 3	0.50	92.89	175	93.05	128
Cavity 4	0.80	93.18	300	93.24	299

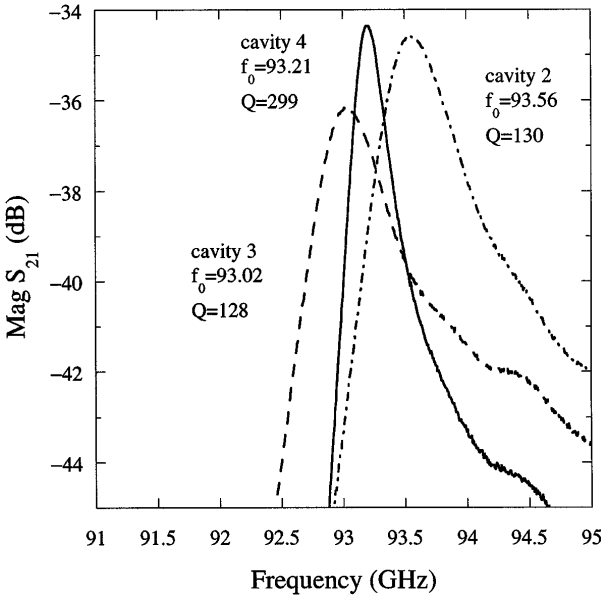

FIG. 1. Cold test transmission spectra, measured in air, for the two intermediate cavities and the output cavity. Cavity 2 response is indicated by the dash-dotted line, cavity 3 by the dashed line, and cavity 4 by the solid line.

for the vacuum dielectric constant, are summarized in Table I.

Upon completion of the cold test, the circuit was installed in the test stand. Figure 2 shows a schematic of the gyroklystron amplifier experiment. A 4 A, 55 kV annular electron beam is produced by a double anode magnetron injection gun. The magnetic field at the cathode, which is nominally 1.5 kG, can be varied to control the beam velocity ratio, $\alpha = \nu_{\mathrm{perp}}/\nu_z$. The beam is adiabatically compressed as it enters the region of high magnetic field generated by the 40 kG superconducting magnet. The four cavities of the gyroklystron circuit are positioned in a region of constant magnetic field. The output cavity tapers up to the collector, which is followed by a quartz vacuum window. A conically shaped, water backed Teflon load is positioned on the atmospheric side of the vacuum window. The temperature rise of the water is used to measure the average rf power. The frequency of the input and output rf signals are measured with a spectrum analyzer. The drive power is supplied by an extended interaction oscillator (EIO), which is mechanically tunable from approximately 92.5 to 95.5 GHz. The drive line between the EIO and input cavity includes two 90° bends in overmoded waveguide and one circular to rectangular transition at the input window. Cold test measurements showed that approximately 40% of drive power is lost between the EIO and the drive cavity. The EIO provides pulses up to 2 μs in duration; the beam and EIO are typically pulsed at 250 Hz for an rf duty cycle of 0.05%.

In the experiment, the beam α and velocity spread were not measured, but were deduced through a combination of theoretical modeling and empirical determination. Studies with an electron trajectory code indicate that beam α's between 1.3 and 1.8, and perpendicular velocity spreads between 4% and 12%, are expected for the nominal operating parameters. In addition, hundreds of measured data points were matched with theoretical predictions assuming a consistent pair of α and perpendicular velocity spread values. For example, the stability of the amplifier circuit was studied. The limiting oscillation was found to be the TE_{011} operating mode in the output cavity. Figure 3 shows the theoretical and experimental start oscillation curves for the TE_{011} mode in cavity 4. For the theory curve, the measured values of resonant frequency Q and beam voltage were used. The beam velocity ratio α was assumed to be 1.5, and perpendicular velocity spread was assumed to be 9%. As shown in Fig. 3, the theoretical curve is in good agreement with experimental results. In addition, the assumed values are consistent with predictions of the electron trajectory code. Theoretical predictions using values of α and velocity spread predicted by the code were successfully matched to many other experimental data points. The good agreement of theory and experiment over a wide range of operating parameters with a consistent pair of α and velocity spread values suggests that these values are valid.

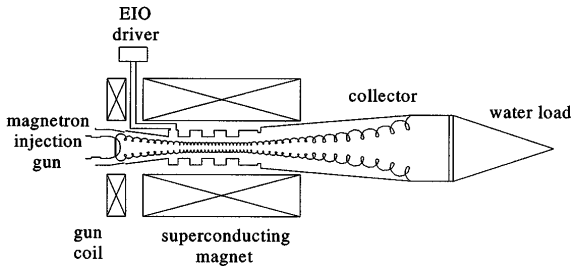

FIG. 2. Schematic of the gyroklystron amplifier test stand.

Figure 4 shows the measured and predicted output power and efficiency as a function of frequency for the amplified TE_{011} mode. A peak saturated output power of 67 kW, corresponding to 28% efficiency, was achieved with a 55 kV, 4.3 A electron beam. The FWHM bandwidth is greater than 460 MHz. The input power measured at the output of the EIO was 87 W, which gives 29 dB saturated gain. Under these operating conditions, the amplifier was unconditionally stable. For the theory curve in Fig. 4, the experimentally determined values of cold resonant frequencies and Q's for the idler and output cavities were used. The HFSS predictions of the drive cavity resonant frequency and Q were assumed. The experimental values of beam voltage, beam current, and magnetic field in the interaction circuit were used. As shown in Fig. 4, the theoretical predictions are in good agreement with experimental data.

Figure 5 shows the measured output power, efficiency, and gain for a slightly reduced beam voltage of 52.6 kV. For the data shown in the figure, the input power is measured at the output of the EIO and the 10 dB loss (4 dB in the drive line and 6 dB in the outer cavity of the input coupler) is not taken into account. The theoretical

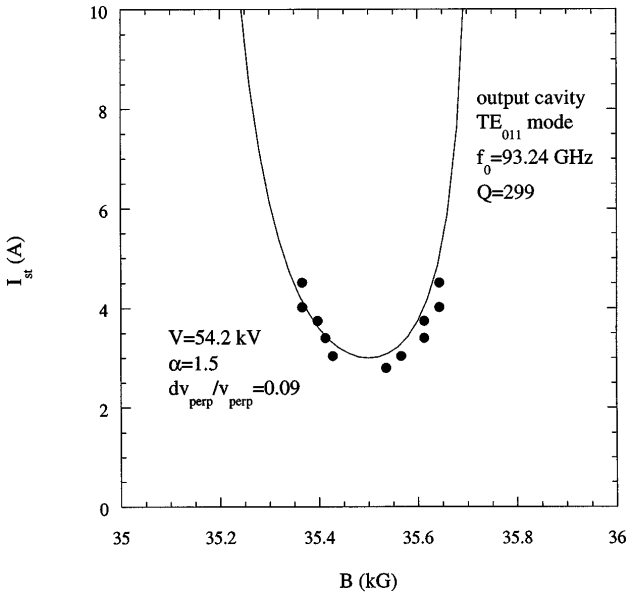

FIG. 3. Experimental and theoretical start oscillation current for the TE_{011} mode in the output cavity. Measured data are indicated by the filled circles, and theoretical predictions are indicated by the solid line.

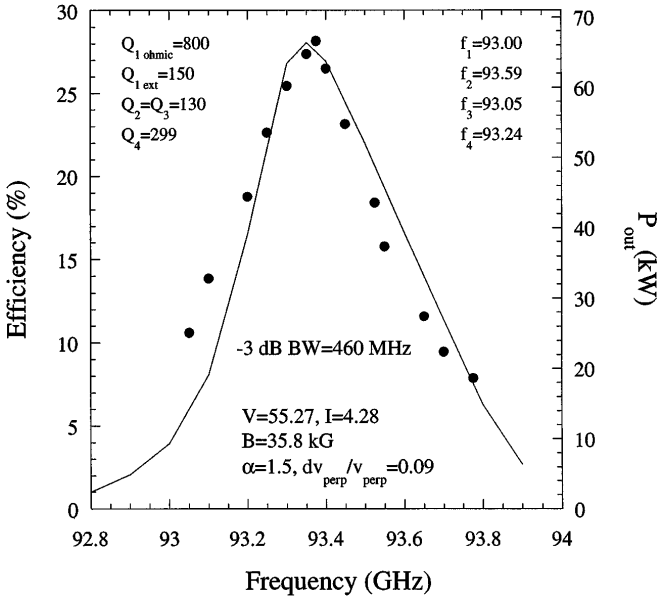

FIG. 4. Experimental and theoretical peak output power versus frequency. Experimental data points are indicated by the filled circles, and theoretical predictions are shown by the solid line.

prediction of efficiency versus input power is also plotted in Fig. 5. For the theory curve, the input power was multiplied by 10 to account for the fact that only 10% of the power leaving the EIO arrives in the TE_{011} mode

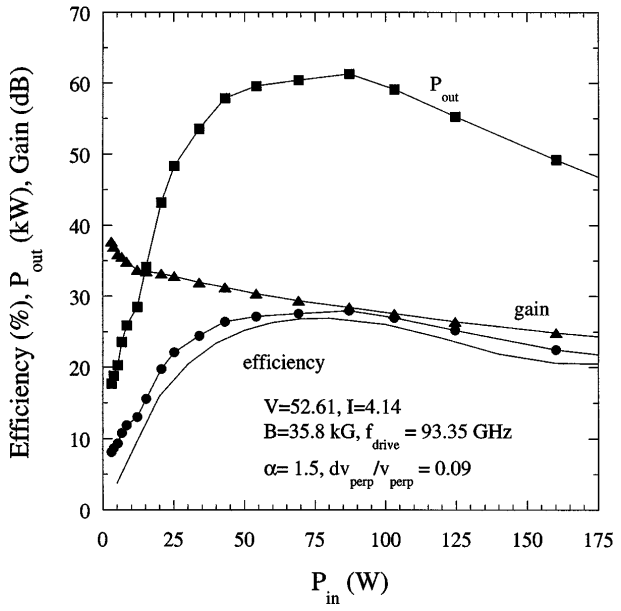

FIG. 5. Experimental and theoretical efficiency, peak output power, and gain versus input power. Measured efficiency points are indicated by the filled circles, measured output power by the filled squares, and measured gain by the filled triangles. The solid line indicates the theoretical prediction of efficiency. For the experimental points, the input power is measured from the EIO output. For the theory curve, the input power is multiplied by 10 to account for the 10 dB loss in the drive line and input cavity.

of the drive cavity. As shown in Fig. 5, the agreement between theory and experiment is good.

In summary, a four cavity *W*-band gyroklystron amplifier circuit was designed, built, and tested. Peak output powers of 67 kW, corresponding to 28% efficiency, were achieved in the TE_{011} mode with a 55 kV, 4.3 A electron beam. The FWHM bandwidth is greater than 460 MHz, a significant increase over the bandwidth demonstrated in previous *W*-band gyroklystron experiments. The small signal and saturated gains are 36 and 29 dB, respectively. The experimental data are in good agreement with predictions of theory using calculated values of beam velocity ratio and velocity spread. The circuit is zero drive stable and the limiting oscillation is the TE_{011} operating mode in the output cavity. Future experiments will focus on increasing bandwidth through more aggressive stagger tuning and reduced output cavity Q.

The authors would like to thank M. Barsanti, F. Robertson, R. Keyser, B. Sobocinski, and M. Ngo for their technical assistance. The authors are grateful to D. Lohrmann for the loan of the EIO driver and to J. Hirshfield for many fruitful discussions. This work was supported by the Office of Naval Research. The computational work was supported in part by a grant of HPC time from the DOD HPC Center NAVO.

*Permanent address: Omega P, Inc., New Haven, CT 06520.

†Permanent address: Mission Research Corp., Newington, VA 22122.

[1] *Applications of High-Power Microwaves*, edited by A. V. Gaponov-Grekhov and V. L. Granatstein (Artech House, Boston, 1994).

[2] L. R. Becerra, G. J. Gerfen, R. J. Temkin, D. J. Single, and R. G. Griffin, Phys. Rev. Lett. **71**, 3561 (1993).

[3] W. M. Bollen, A. H. McCurdy, B. Arfin, R. K. Parker, and A. K. Ganguly, IEEE Trans. Plasma Sci. **13**, 417 (1985).

[4] E. V. Zasypkin, M. A. Moiseev, E. V. Sokolov, and V. K. Yulpatov, Int. J. Electron. **78**, 423 (1995).

[5] W. G. Lawson *et al.*, Phys. Rev. Lett. **67**, 520 (1991).

[6] H. W. Matthews *et al.*, IEEE Trans. Plasma Sci. **22**, 825 (1994).

[7] H. R. Jory, F. Freidlander, S. J. Hegji, J. R. Shively, and R. S. Symons, IEDM Technical Digest 234 (1977).

[8] E. V. Zasypkin, M. A. Moiseev, I. G. Gachev, and I. I. Antakov, IEEE Trans. Plasma Sci. **24**, 666 (1996).

[9] I. I. Antakov, E. V. Zasypkin, and E. V. Sokolov, Proc. SPIE Int. Soc. Opt. Eng. **2104**, 166 (1993).

[10] R. P. Fischer *et al.*, Phys. Rev. Lett. **72**, 2395 (1994).

[11] P. E. Latham, W. Lawson, and V. Irwin, IEEE Trans. Plasma Sci. **22**, 804 (1994).

[12] J. M. Neilson, P. E. Latham, M. Caplan, and W. Lawson, IEEE Trans. Microwave Theory Tech. **37**, 1165 (1989).

[13] G. S. Park, C. M. Armstrong, R. H. Kyser, J. L. Hirshfield, and R. K. Parker, Int. J. Electron. **78**, 983 (1995).

[14] P. E. Latham, S. M. Miller, and C. D. Striffler, Phys. Rev. A **45**, 1197 (1992).